THE JOURNAL OF PHYSICAL CHEMISTRY Letters

pubs.acs.org/JPCL

# Analysis of the Size Distribution of Single-Walled Carbon Nanotubes Using Optical Absorption Spectroscopy

Ying Tian,[†] Hua Jiang,[†] Jan v. Pfaler,[‡] Zhen Zhu,[†] Albert G. Nasibulin,*[,†] Timur Nikitin,[§] Brad Aitchison,[⊥] Leonid Khriachtchev,[§] David P. Brown,[⊥] and Esko I. Kauppinen*[,†,#]

[†]NanoMaterials Group, Department of Applied Physics and Center for New Materials, Aalto University, Puumiehenkuja 2, 00076, Finland, [‡]Department of Mathematics and Systems analysis, Aalto University, Espoo, Finland, [§]Department of Chemistry, University of Helsinki, P.O. Box 55, 00014 Helsinki, Finland, [⊥]Canatu Ltd, 02150, Espoo, Finland, and [#]VTT Biotechnology, Espoo, Finland

**ABSTRACT** The diameter of single-walled carbon nanotubes (SWNTs) is an important characteristic to determine their electronic properties and direct further applications in electronics and photonics. A demand currently exists for an accurate and rapid method of evaluating the mean diameter and diameter distribution of bulk SWNTs. Here, we provide an effective means for quantifying the diameter distribution of SWNTs using optical absorption spectroscopy without a strict prior assumption on the form of the diameter distribution. Verification of this assignment protocol is based upon statistical analysis of hundreds of high-resolution transmission electron microscopy (HRTEM) images as well as comparison with Raman measurements on the same SWNT samples. A good agreement among different techniques indicates that this approach enables accurate and rapid assessment of diameter distribution and can be extended to bulk SWNT samples with various diameter distributions.

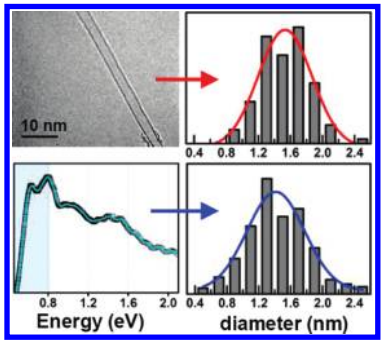


SECTION Nanoparticles and Nanostructures

Single-walled carbon nanotubes have attracted intense interest due to their unique electronic, optical, thermal, and mechanical properties useful for various applications.[1] The diameter and chiral angle of a SWNT fully define the geometric structure and electronic properties, which are central for their applications to electronics and photonics. Although many synthesis techniques of SWNTs have been successfully developed (arc discharge, laser desorption, and chemical vapor deposition (CVD)), in all known fabrication methods, the SWNTs are produced simultaneously in various diameters and chiral angles. Therefore, it is critical to develop an efficient method which provides reliable characterization of the produced SWNTs in order to properly understand their basic electronic and optical behaviors and for subsequent implementation in nanotube-based applications.

TEM[2,3] and electron diffraction (ED)[4,5] of individual SWNTs have been applied to provide direct analysis of both diameter and chiral angles without ambiguity. HRTEM allows us to observe directly the structure of SWNTs without relying on physical properties or modeling. This has proven to be the only reliable technique to obtain populations of SWNT characteristics.[2,3] However, a problem common to the electron microscopy technique is its low efficiency in obtaining a diameter distribution on bulk SWNTs.

In contrast to the direct analysis methods, Raman spectroscopy as a bulk sensitive method has been widely used to characterize the diameter of SWNTs based on the reverse relationship between the diameter and the frequency of radial breathing modes (RBMs). The Raman response for this mode strongly depends upon the laser excitation energy; thus, several laser lines are required to estimate the mean diameter and diameter distribution of a bulk SWNT sample.[6] Complementary to Raman spectroscopy, optical absorption spectrometry has been proven to be a powerful tool to evaluate these properties of a bulk SWNT sample since all types of nanotubes are active in the UV−vis−NIR region.[7] However, the evaluation of mean diameter and diameter distributions very much depend on the model used to analyze the data. In addition, the diameter distribution of a bulk SWNT sample is typically assumed a priori to be Gaussian.[7−11] However, SWNTs produced via the CVD and HiPCO processes often cannot be accurately approximated by a simple diameter distribution.[7,9,10] Consequently, the absorption spectra do not necessarily show the three well-resolved main absorption peaks that correspond to the first and second transition energies of semiconducting nanotubes ($E_{11}^{S}$, $E_{22}^{S}$) and the first transition energy of metallic nanotubes ($E_{11}^{M}$). In such a case, it is impractical to follow a canonical approach by which one first identifies the absorption peaks and then assigns each to a specific transition energy.[7−15]

In the present work, we determine the mean diameters and diameter distributions of bulk SWNTs by means of

**Received Date:** February 5, 2010
**Accepted Date:** March 15, 2010



DOI: 10.1021/jz100161p | *J. Phys. Chem. Lett.* **2010**, *1*, 1143–1148

Raman and optical absorption spectroscopy in combination with the direct observation technique by electron microscopy. We introduce a universal method for more effective assignment of diameter distributions from the optical absorption spectrum without making a strict assumption regarding the form of the diameter distribution. This method can be used as a versatile tool to analyze absorption spectra regardless of the form or overlap of the absorption bands. The resulting diameter distributions were further compared with Raman measurements and validated based on statistical analysis of hundreds of HRTEM images performed on the same SWNT samples.

The SWNT samples were synthesized by a scale-up aerosol reactor using ferrocene as the catalyst precursor and CO as the carbon source.[16,17] $CO_2$ plays an important role in the growth process.[18] SWNTs with different mean diameters and diameter distributions were synthesized at 920 °C with different concentrations of added $CO_2$ (denoted C1, C2, C3, C4, and C5 for $CO_2$ concentrations of 0, 0.4, 0.7, 1.0, and 1.2%, respectively). Figure 1 shows the Raman spectra of the as-prepared samples using excitation energies of 1.58, 2.33, and 2.54 eV. As expected, the Raman spectra of the samples exhibited strong G bands (Figure 1a) and RBM features (Figure 1b, c, and d), with the exception of sample S5, which had very low-intensity G and RBM bands, indicating that there is little carbon nanotube material and substantial amounts of impurities. Similar results were observed by TEM measurement (Figure S1, Supporting Information).

The RBMs correspond to the coherent vibration of the carbon atoms in the radial direction and are used to probe the nanotube diameter ($d_t$) by the well-established relationship of $d_t = A/\omega_{RBM} + B$, where $A = 217.8$ and $B = 15.7$ are determined experimentally.[19,20] When the 2.33 eV laser is applied (Figure 1b), the RBMs are similarly positioned in these samples. However, the relative intensity at a higher frequency range of 200−270 $cm^{-1}$ steadily decreases as the $CO_2$ concentration increases. This indicates that the relative abundance of smaller-diameter nanotubes decreases with increasing $CO_2$ concentration.

Figure 1c and d shows the RBM regions of SWNT samples using the excitation energies 1.58 and 2.54 eV, respectively. Similarly, the relative intensity of the RBMs at the higher frequencies (indicated in the dashed frame) decrease with increasing $CO_2$ concentration. Again, this corresponds to a diminishing fraction of smaller-diameter SWNTs and thus an increase in the mean diameter.

Plotting the optical transition energy $E_{ii}$ against the RBM frequency, using the Kataura plot,[21,22] one can assign the RBM peaks to particular chiralities (or at least to particular $2n + m$ families). The Kataura plot used in the present study (Figure S3, Supporting Information) is calculated by the extended tight-binding model (ETB), which takes into account rehybridization of $\sigma$ and $\pi$ orbitals induced by the curvature of the SWNT sidewall and long-range atomic interactions.[23] After the geometrical structure optimization,[24] the many-body corrections including both exciton binding energy and the coulomb self-energy are further applied by using logarithmic corrections with empirical parameters.[25,26] Here, the model is denoted by ETB/MB. It is worth noting that the mechanism

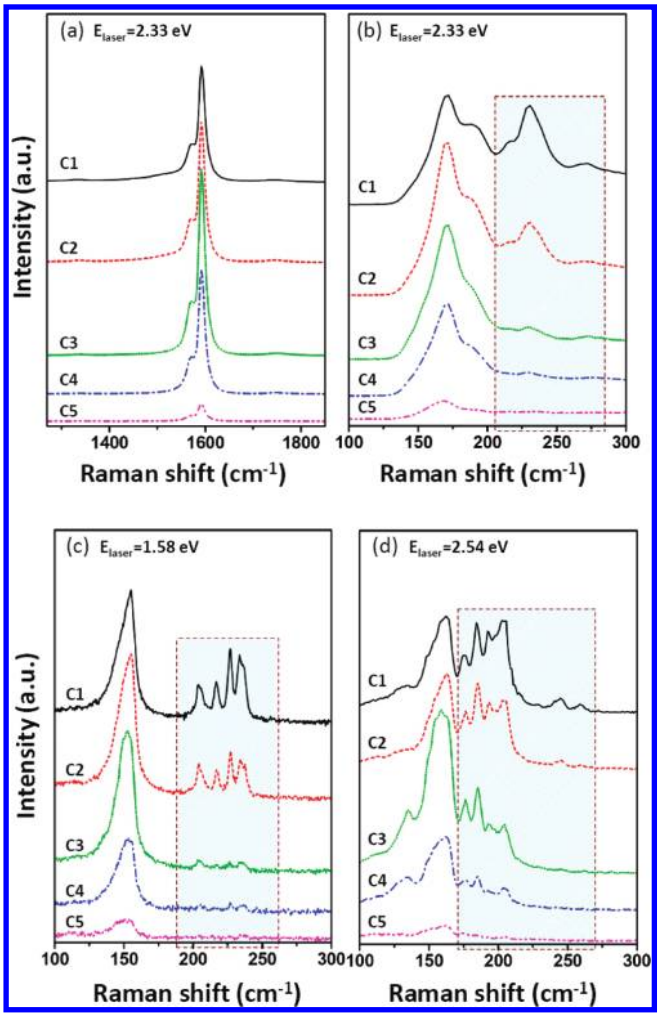


**Figure 1.** Raman spectra of SWNT samples synthesized at 920 °C with different $CO_2$ concentrations excited by various laser energies. (a) G, D bands and (b) the RBMs at 2.33 eV laser energy and the RBM spectra using lasers of (c) 1.58 and (d) 2.54 eV, respectively.

previously used for band to band transitions between van Hove singularities (VHs) is still applicable for the exciton picture from the ETB/MB model.[27] Detailed assignments are discussed and listed in Table S1 (Supporting Information). The very small differences between theoretical and experimental values indicate that the Kataura plot based on the ETB/MB model is accurate enough to analyze the SWNT thin-film samples in the present study.

Although Raman spectroscopy is a useful tool to characterize the diameters of SWNTs, it is still challenging to obtain an accurate diameter distribution of SWNTs from the resonant Raman data. However, the UV−vis−NIR absorption spectrometer can be distinguished as a technique which can quickly and effectively provide valuable information on the overall diameter distribution of SWNTs. Figure 2a shows the as-measured absorption spectra of the SWNT thin-film samples. We note that the baselines of the spectra have been vertically translated for clarity. The absorption peaks from interband electronic transitions, shown in the enlarged low-energy



DOI: 10.1021/jz100161p | J. Phys. Chem. Lett. 2010, 1, 1143–1148

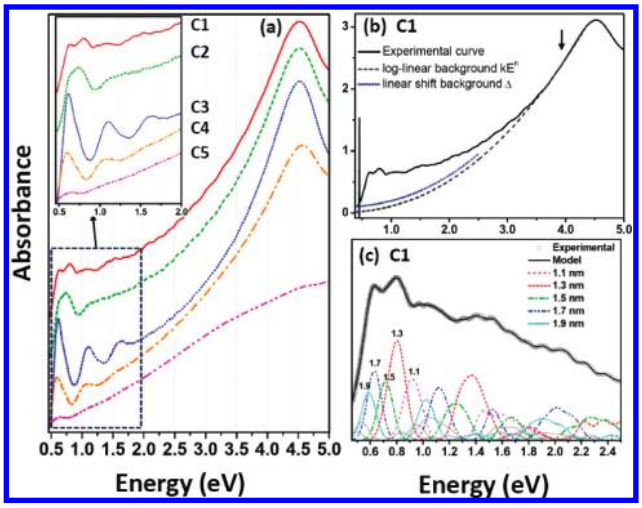


**Figure 2.** (a) The absorption spectra of SWNT samples synthesized at 920 °C with different $CO_2$ concentrations. (b) The absorption spectra of sample C1 along with nonlinear and linear shifts of the backgrounds are shown as dashed and dotted lines, respectively. The arrow depicts the data region where the background was generated. (c) The absorption spectrum of sample C1 after background subtraction (dotted gray line) and the corresponding calculated absorption spectrum (solid gray line). The contributions from the labeled diameter groups of SWNTs are denoted by the colored dashed lines under the absorption peaks areas.

region, strongly overlap in samples C1 and C2. The absorption peaks become more resolved and narrower for the samples collected at higher $CO_2$ concentrations, which corresponds to a narrower diameter distribution in these samples. Moreover, the first absorption peak from $E_{11}^S$ was observed to shift to lower energy (implying a larger mean diameter) from C2 to C4 (from top to bottom). For sample C1, the absorption peak from $E_{11}^S$ shows a bimodal structure where a peak cannot be identified. The rather flat feature in the absorption spectrum from sample C5 confirms the observation that the SWNT fraction in C5 is low, which has been verified by Raman analysis (Figure 1) and TEM imaging (Figure S1, Supporting Information).

The absorption spectra of the bulk SWNT samples in ref 7, 8, and 11−14 typically showed three pronounced absorption peaks, starting from the lowest energy, corresponding to $E_{11}^S$, $E_{22}^S$, and $E_{11}^M$, respectively. The simple tight-binding model[21] has been often used to predict the energy band gaps of semiconducting and metallic nanotubes, which depend on the diameter $E_{11}^S = 2a_0\gamma_0/d_t$, $E_{22}^S = 4a_0\gamma_0/d_t$, and $E_{11}^M = 6a_0\gamma_0/d_t$, where $\gamma_0$ is interaction energy between neighboring C atoms and $a_0$ is the C−C bond distance. However, this model does not consider the curvature and many-body effects which were found to be quite strong in the one-dimensional nanotube system.[28] From the analysis of RBM peaks in the Raman spectra, the ETB/MB model (Figure S2, Supporting Information) shows very good agreement with the experimental results. Thus, for the same SWNT thin-film samples, it is reasonable to use this model as a base for the optical absorption analysis.

The total absorption profile can be assumed to be a linear composition of background absorption and contributions from the SWNT material in the thin-film sample according to

$$A(E) = A_{bg}(E) + A_{SWNT}(E) \quad (1)$$

where $A_{bg}(E)$ is background absorption due to graphite, catalyst particles scattering, and $\pi$-plasma absorption of carbonaceous material.[15,29,30] Although a number of attempts have been made to utilize a linear background model,[7,11,31,32] a nonlinear function would better account for physical properties in the SWNTabsorption spectrum such as peak overlap and transition broadening.[33]

We analyze the background absorption in two parts, which can be written as

$$A_{bg}(E) = kE^n + \Delta \quad (2)$$

where

$$\Delta = \frac{\omega_a(E_U - E) + \omega_b(E_L - E)}{E_U - E_L} \quad (3)$$

First, the log-linear model[15,30] is applied to simulate the nonlinear part $kE^n$ of the background absorption. Then, a small positive linear shift $\Delta$ of the background and parameters in $A_{SWNT}(E)$ is fitted. Parameters $k$ and $n$ are empirical, and the remaining parameters $\omega = \omega_a, \omega_b, \ldots, \omega_{n,m}, \ldots$ are estimated based on the absorption in the range from $E_L = 0.46$ eV to $E_U = 2.50$ eV. The result of the above process is displayed in Figure 2b for sample C1. More detailed discussions about background subtraction are provided in the Supporting Information.

After background subtraction, the absorbance is assumed to be essentially only due to the interband electronic transitions of the SWNT material. We model optical absorption as a linear composition of each nanotube type

$$A_{SWNT}(E) = \sum_{(n,m)} \omega_{(n,m)} A_{(n,m)}(E) \quad (4)$$

Here, $\omega_{(n,m)}$ reflects the absorption probability of the $(n,m)$-SWNT in the bulk ($n \geq m \geq 0$). We interpret $C_{(n,m)} = \omega_{(n,m)}/\sum_{(n,m)}\omega_{(n,m)}$ as a proxy for proportion of the $(n,m)$-SWNT in the sample. $A_{(n,m)}(E)$ is the characteristic absorption spectrum of $(n,m)$ tubes. This is assumed to be a sum of Gaussian line shapes describing the broadening of each optical transition due to the finite lifetime and finite resolution of the spectrometer

$$A_{(n,m)}(E) = \sum_i \exp\left[-\frac{1}{2}\left(\frac{E - E_{(n,m)}^{ii}}{\Delta E}\right)^2\right] \quad (5)$$

The broadening factor ($\Delta E = 50$ meV), tested from 20 to 80 meV, was found not to be a crucial parameter for the final results. The transition energy $E_{(n,m)}^{ii}$ ($i = 1, 2, 3, \ldots$) was taken from ETB/MB theory. For large-diameter semiconducting nanotubes ($d_t > 1.5$ nm), the higher transition energies of $E_{33}^S$ and $E_{44}^S$ are already less than 2.5 eV (shown in the Kataura plot) and will contribute to the overall absorption spectra. Thus all of the transition energies within the fitting scale ($E_L - E_U$) were considered in the calculation. For metallic nanotubes, the transition energies split except for the armchair nanotubes due to the trigonal warping effect.[34] The higher and lower branches correspond to the $E_{11H}^M$ and $E_{11L}^M$ transitions, respectively. The optical transition corresponding to $E_{11H}^M$ was



DOI: 10.1021/jz100161p | J. Phys. Chem. Lett. 2010, 1, 1143–1148

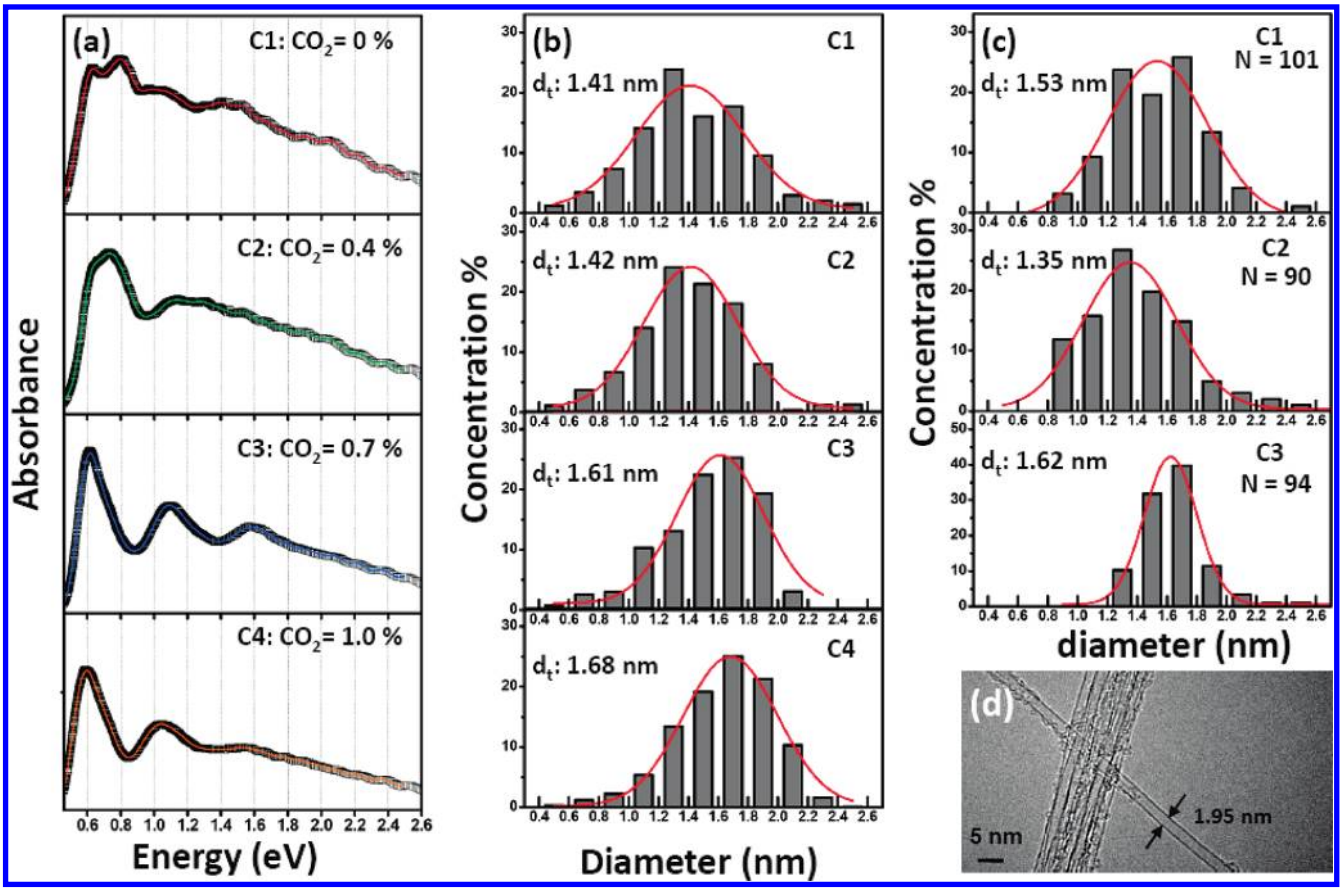


**Figure 3.** (a) The absorption spectra after background subtraction (black dots) and the fitted curves (solid lines) of the SWNT samples. (b) The fitted diameter distribution of SWNT samples based on absorption spectra, which give mean diameters $d_t$ of samples C1, C2, C3, and C4 of 1.41, 1.42, 1.61, and 1.68 nm, respectively. (c) The diameter distributions of SWNT samples of C1, C2, and C3 measured from high-resolution TEM images. Red solid lines correspond to the Gaussian fits which give the $d_t$ of 1.53, 1.35, and 1.62 nm, respectively. (d) An example of a HRTEM image taken from sample C1.

recently observed in Raman studies, but the intensity associated with $E_{11\mathrm{H}}^{\mathrm{M}}$ was much lower than that to $E_{11\mathrm{L}}^{\mathrm{M}}$ transitions.[22] In addition, SWNTs, as known, prefer to grow in the armchair direction. Therefore, we have reasons not to consider the contribution of $E_{11\mathrm{H}}^{\mathrm{M}}$ transitions of metallic nanotubes in the optical absorption process. We assume that the broadening factors and absorption cross sections were both independent of the SWNT chiralities or different interband transitions. The nanotubes whose diameters were in the scale of 0.5−2.5 nm were considered in the fitting process.

The direct linear problem of finding the coefficients $\omega = \omega_a, \omega_b, \ldots, \omega_{n,m}, \ldots$ is highly ill-conditioned. A well-conditioned basis $\{A_{n,m}\}$ can, at most, contain on the order of 40 such vectors ($E_U - E_L = 2$ eV, $\Delta E = 50$ meV). Hence, the problem is not solvable without an additional assumption, nor can we expect to solve any one weight accurately. Rather, we should aim at a consistent distribution under reasonable — and as least restrictive as possible — a priori assumptions. Consequently, we propose using a regularization scheme

$$\min_{\omega} \| A(\omega) - A_{\mathrm{measured}} \|_2^2 + c\Phi(\omega) \qquad (6)$$

Here, we considered two approaches for $\Phi(\omega)$; the weights of "similar" SWNTs are correlated, $\Phi(\omega) = \omega^{\mathrm{T}} C \omega$, where $C$ is a positive definite correlation matrix, or that the special case using 2-norm, $\Phi(\omega) = \| \omega \|_2^2$. Note that, although both impose an assumption on the SWNT distribution, they are much less limiting assumptions than imposing a Gaussian distribution on the diameter. We resort here to the latter approach as we found it produce rather satisfactory results with simpler assumptions. Clearly, the regularization parameter $c > 0$ needs to be chosen to produce reasonable results. We found that $c$ values in the range from 1 to 3 typically achieve this.

As shown in Figure 3a, the dotted black lines represent the original absorption spectra after the background subtraction, and the thin solid lines on the top denote the fitted spectra. Very small differences were observed between the fitted spectra and the experimental absorption spectra. The associated diameter distributions of the calculated spectra are drawn in the Figure 3b. For sample C1, the diameter histogram showed a bimodal distribution, with the most abundant diameters of SWNTs centered at 1.3 and 1.7 nm. The detailed deconvolution of absorption peak areas by different diameter groups of SWNTs is represented by the colored dashed curves in Figure 2c. The calculated mean diameter is 1.41 nm. More than 80% of the tubes were determined to be in the diameter distribution of 1.0−2.0 nm. After adding a small amount of



DOI: 10.1021/jz100161p | J. Phys. Chem. Lett. 2010, 1, 1143–1148

$CO_2$, the bimodal diameter distribution merged to a single distribution. Sample C2 shows a mean diameter $d_t$ of 1.42 nm, and approximately 78% of the nanotubes are in the range from 1.0 to 1.8 nm in diameter. By continuously increasing the $CO_2$ concentration, the mean diameter of sample C3 is shifted to 1.61 nm, with a much lower fraction of small-diameter nanotubes produced. For sample C4, the mean diameter further increased to 1.68 nm, with 89% of the nanotubes ranging from 1.2 to 2.0 nm in diameter. The results, based on absorption spectra, are in good agreement with the initial Raman studies, that is, the relative abundance of smaller-diameter decreases with the increase of $CO_2$ concentration, which results in a narrower diameter distribution and an increase in the mean diameter.

The nanotube diameter distributions assessed by the above spectroscopy measurements have been validated by using high-resolution TEM, which allows direct observation and quantitative characterization of the nanotube structures. For this purpose, about 100 randomly isolated SWNTs from each sample (C1, C2, and C3) were imaged. The microscope was carefully calibrated with a standard sample (Au particles) for the magnification that was used in this work. In order to minimize the ambiguity of the measurement due to the focusing deviations resulting from the possible variance in the sample height, all images were focused by adjusting the heights of the specimens while keeping the current of the objective lens constant. HRTEM images were taken under such a focusing condition that the two walls of a nanotube produced two sharpest dark lines. Under these conditions, the accuracy of the diameter measurements from HRTEM is estimated to be about ±0.1 nm.

Figure 3d shows an example of a diameter measurement from a HRTEM image taken from sample C1. The diameter histograms of the SWNT samples measured from HRTEM images are plotted in Figure 3c. For sample C1, a Gaussian fit showed a mean diameter of 1.53 nm, with 90% of the SWNTs in the diameter range of 1.0−2.0 nm. The deduced diameter histogram shows SWNTs centered at 1.3 and 1.5 nm in diameter. This is in good agreement with the results obtained from absorption spectra analysis. Compared with the Raman results in Figure 1 and Table S1 (Supporting Information), using different laser lines, all of the RBMs spectra, indeed, showed that sample C1 had the highest relative population of smaller-diameter nanotubes (from 1.0 to 1.4 nm), which again supports the possibility of bimodal diameter distribution. For samples C2 and C3, the diameter diagrams derived from the HRTEM measurements yield mean diameters of 1.35 and 1.62 nm, respectively, which is consistent with the results obtained from absorption spectra, that is, 1.42 and 1.61 nm, respectively. Additionally, there is a good agreement with the diameter distributions in samples C2 and C3. More than 77% of the SWNTs in sample C2 have diameters in the range of 1.0−1.8 nm, and in sample C3, about 90% of the SWNTs are from 1.2 to 2.0 nm in diameter.

In summary, by a combination of spectroscopic and microscopic techniques, we have successfully determined the mean diameters and properties of diameter distributions of as-synthesized SWNT bulk samples. A novel method was developed for more efficient evaluation of the mean diameter and diameter distribution of a bulk SWNT sample from optical absorption spectra. Without making a strict assumption for the form of the diameter distribution, the optical absorption from the transition energies of each nanotube was modeled by summing contributions over the entire absorption spectrum. The transition energies of a SWNT are described by a sum of Gaussian line shapes and known peak positions corresponding to the ETB/MB model, which was verified by Raman spectroscopy on the same bulk SWNTs. The highly ill-posed problem was well-resolved by the introduction of a regularization term in the fitting process. Raman spectroscopy and high-resolution transmission electron microscopy techniques were employed to validate the results. Comparisons between different techniques suggested that absorption spectroscopy of bulk SWNTs is very efficient in assessing diameter distributions regardless of the appearance of absorption bands and forms of diameter distributions. In addition, the biomodal diameter distribution of SWNTs is regarded as a consequence from the continuous decomposition of ferrocene throughout the reactor at the set temperature. Meanwhile, the results of diameter distributions imply that $CO_2$ as an etching agent plays an important role in tailoring diameters of SWNTs. The growth mechanisms will be addressed in detail in a separate publication.

**SUPPORTING INFORMATION AVAILABLE** Experimental details of sample characterization; TEM image of sample C5; detailed assignments of ($n$,$m$) chiralities or families (Table S1) from the RBM region of Raman spectra based on the Kataura plot (Figure S2); and discussions about background subtraction. This material is available free of charge via the Internet at http://pubs.acs.org.

## AUTHOR INFORMATION

### Corresponding Author:

*To whom correspondence should be addressed. E-mail: albert.nasibulin@tkk.fi (A.G.N.); esko.kauppinen@tkk.fi (E.I.K.). Fax: +358 924513517. Tel: +358 405098064.

**ACKNOWLEDGMENT** We are grateful to Jussi O. Sarkkinen for his help with experiments. This work was financially supported by the Academy of Finland (Projects 128495 and 128445), TEKES (GROCO and NaBuFi projects), and the CNB-E project in the Aalto University Multidisciplinary Institute of Digitalization and Energy (MIDE) Programme. T.N. and L.K. acknowledge the Finnish Centre of Excellence in Computational Molecular Science and the FinNano Program (OPNA).

## REFERENCES

(1) Dresselhaus, M. S.; Dresselhaus, G.; Avouris, P. *Carbon Nanotubes Synthesis, Structures, and Applications*; Springer: New York, 2001.

(2) Sato, Y.; Yanagi, K.; Miyata, Y.; Suenaga, K.; Kataura, H.; Iijima, S. Chiral-Angle Distribution for Separated Single-Walled Carbon Nanotubes. *Nano Lett.* **2008,** *8*, 3151–3154.

(3) Fleurier, R.; Lauret, J.-S.; Lopez, U.; Loiseau, A. Transmission Electron Microscopy and UV−Vis−IR Spectroscopy Analysis of the Diameter Sorting of Carbon Nanotubes by Gradient Density Ultracentrifugation. *Adv. Funct. Mater.* **2009,** *19*, 2219–2223.

(4) Jiang, H.; Brown, D. P.; Nasibulin, A. G.; Kauppinen, E. I. Robust Bessel-Function-Based Method for Determination of



DOI: 10.1021/jz100161p | *J. Phys. Chem. Lett.* **2010,** *1*, 1143–1148

the (*n*,*m*) Indices of Single-Walled Carbon Nanotubes by Electron Diffraction. *Phys. Rev. B* **2006,** *74*, 035427–035435.

(5) Meyer, J. C.; Paillet, M.; Duesberg, G. S.; Roth, S. Electron Diffraction Analysis of Individual Single-Walled Carbon Nanotubes. *Ultramicroscopy* **2006,** *106*, 176–190.

(6) Rao, A. M.; Richter, E.; Bandow, S.; Chase, B.; Eklund, P. C.; Williams, K. A.; Fang, S.; Subbaswamy, K. R.; Menon, M.; Thess, A.; Smalley, R. E.; Dresselhaus, G.; Dresselhaus, M. S. Diameter-Selective Raman Scattering from Vibrational Modes in Carbon Nanotubes. *Science* **1997,** *275*, 187–191.

(7) Liu, X.; Pichler, T.; Knupfer, M.; Golden, M. S.; Fink, J.; Kataura, H.; Achiba, Y. Detailed Analysis of the Mean Diameter and Diameter Distribution of Single-Wall Carbon Nanotubes from Their Optical Response. *Phys. Rev. B* **2002,** *66*, 045411–045419.

(8) Selbmann, D.; Bendjemil, B.; Leonhardt, A.; Pichler, T.; Täschner, C.; Ritschel, M. A Parametric Study of the Synthesis and Purification of Single-Walled Carbon Nanotubes Using the High-Pressure Carbon Monoxide Process. *Appl. Phys. A* **2008,** *90*, 637–643.

(9) Nikolaev, P.; Bronikowski, M. J.; Bradley, R. K.; Rohmund, F.; Colbert, D. T.; Smith, K. A.; Smalley, R. E. Gas-Phase Catalytic Growth of Single-Walled Carbon Nanotubes from Carbon Monoxide. *Chem. Phys. Lett.* **1999,** *313*, 91–97.

(10) Bhowmick, R.; Clemens, B. M.; Cruden, B. A. Parametric Analysis of Chirality Families and Diameter Distributions in Single-Wall Carbon Nanotube Production by the Floating Catalyst Method. *Carbon* **2008,** *46*, 907–922.

(11) Barreiro, A.; Kramberger, C.; Rümmeli, M. H.; Grüneis, A.; Grimm, D.; Hampel, S.; Gemming, T.; Büchner, B.; Bachtold, A.; Pichler, T. Control of the Single-Wall Carbon Nanotube Mean Diameter in Sulphur Promoted Aerosol-Assisted Chemical Vapour Deposition. *Carbon* **2007,** *45*, 55–61.

(12) Ichida, M.; Mizuno, S.; Saito, Y.; Kataura, H.; Achiba, Y.; Nakamura, A. Coulomb Effects on the Fundamental Optical Transition in Semiconducting Single-Walled Carbon Nanotubes: Divergent Behavior in the Small-Diameter Limit. *Phys. Rev. B* **2002,** *65*, 241407–241411.

(13) Lin, X.; Rümmeli, M. H.; Gemming, T.; Pichler, T.; Valentin, D.; Ruani, G.; Taliani, C. Single-Wall Carbon Nanotubes Prepared with Different Kinds of Ni−Co Catalysts: Raman and Optical Spectrum Analysis. *Carbon* **2007,** *45*, 196–202.

(14) Wiltshire, J. G.; Li, L.-J.; Herz, L. M.; Nicholas, R. J.; Glerup, M.; Sauvajol, J.-L.; Khlobystov, A. N. Chirality-Dependent Boron-Mediated Growth of Nitrogen-Doped Single-Walled Carbon Nanotubes. *Phys. Rev. B* **2005,** *72*, 205431–205437.

(15) Ryabenko, A. G.; Dorofeeva, T. V.; Zvereva, G. I. Uv-Vis-Nir Spectroscopy Study of Sensitivity of Single-Wall Carbon Nanotubes to Chemical Processing and Van-Der-Waals SWNT/SWNT Interaction. Verification of the SWNT Content Measurements by Absorption Spectroscopy. *Carbon* **2004,** *42*, 1523–1535.

(16) Moisala, A.; Nasibulin, A. G.; Shandakov, S. D.; Jiang, H.; Kauppinen, E. I. On-Line Detection of Single-Walled Carbon Nanotube Formation During Aerosol Synthesis Methods. *Carbon* **2005,** *43*, 2066–2074.

(17) Moisala, A.; Nasibulin, A. G.; Brown, D. P.; Jiang, H.; Khriachtchev, L.; Kauppinen, E. I. Single-Walled Carbon Nanotube Synthesis Using Ferrocene and Iron Pentacarbonyl in a Laminar Flow Reactor. *Chem. Eng. Sci.* **2006,** *61*, 4393–4402.

(18) Nasibulin, A. G.; Brown, D. P.; Queipo, P.; Gonzalez, D.; Jiang, H.; Kauppinen, E. I. An Essential Role of $CO_2$ and $H_2O$ During Single-Walled CNT Synthesis from Carbon Monoxide. *Chem. Phys. Lett.* **2006,** *417*, 179–184.

(19) Dresselhaus, M. S.; Dresselhaus, G.; Saito, R.; Jorio, A. Raman Spectroscopy of Carbon Nanotubes. *Phys. Rep.* **2005,** *409*, 47–99.

(20) Araujo, P. T.; Doorn, S. K.; Kilina, S.; Tretiak, S.; Einarsson, E.; Maruyama, S.; Chacham, H.; Pimenta, M. A.; Jorio, A. Third and Fourth Optical Transitions in Semiconducting Carbon Nanotubes. *Phys. Rev. Lett.* **2007,** *98*, 067401–067404.

(21) Kataura, H.; Kumazawa, Y.; Maniwa, Y.; Umezu, I.; Suzuki, S.; Ohtsuka, Y.; Achiba, Y. Optical Properties of Single-Wall Carbon Nanotubes. *Synth. Met.* **1999,** *103*, 2555–2558.

(22) Son, H.; Reina, A.; Samsonidze, G. G.; Saito, R.; Jorio, A.; Dresselhaus, M. S.; Kong, J. Raman Characterization of Electronic Transition Energies of Metallic Single-Wall Carbon Nanotubes. *Phys. Rev. B* **2006,** *74*, 073406–073404.

(23) Valentin, N. P. Curvature Effects on the Structural, Electronic and Optical Properties of Isolated Single-Walled Carbon Nanotubes within a Symmetry-Adapted Non-Orthogonal Tight-Binding Model. *New J. Phys* **2004,** *6*, 17–34.

(24) Samsonidze, G. G.; Saito, R.; Kobayashi, N.; Gruneis, A.; Jiang, J.; Jorio, A.; Chou, S. G.; Dresselhaus, G.; Dresselhaus, M. S. Family Behavior of the Optical Transition Energies in Single-Wall Carbon Nanotubes of Smaller Diameters. *Appl. Phys. Lett.* **2004,** *85*, 5703–5705.

(25) Kane, C. L.; Mele, E. J. Electron Interactions and Scaling Relations for Optical Excitations in Carbon Nanotubes. *Phys. Rev. Lett.* **2004,** *93*, 197402–197406.

(26) Fantini, C.; Jorio, A.; Souza, M.; Strano, M. S.; Dresselhaus, M. S.; Pimenta, M. A. Optical Transition Energies for Carbon Nanotubes from Resonant Raman Spectroscopy: Environment and Temperature Effects. *Phys. Rev. Lett.* **2004,** *93*, 147406–147410.

(27) Filho, A. G. S.; Endo, M.; Muramatsu, H.; Hayashi, T.; Kim, Y. A.; Barros, E. B.; Akuzawa, N.; Samsonidze, G. G.; Saito, R.; Dresselhaus, M. S. Resonance Raman Scattering Studies in $Br_2$-Adsorbed Double-Wall Carbon Nanotubes. *Phys. Rev. B* **2006,** *73*, 235413–235425.

(28) Maultzsch, J.; Pomraenke, R.; Reich, S.; Chang, E.; Prezzi, D.; Ruini, A.; Molinari, E.; Strano, M. S.; Thomsen, C.; Lienau, C. Exciton Binding Energies in Carbon Nanotubes from Two-Photon Photoluminescence. *Phys. Rev. B* **2005,** *72*, 241402–241406.

(29) Lin, M. F.; Shung, K. W. K. Plasmons and Optical Properties of Carbon Nanotubes. *Phys. Rev. B* **1994,** *50*, 17744–17747.

(30) Nair, N.; Usrey, M. L.; Kim, W.-J.; Braatz, R. D.; Strano, M. S. Estimation of the (*n*,*m*) Concentration Distribution of Single-Walled Carbon Nanotubes from Photoabsorption Spectra. *Anal. Chem.* **2006,** *78*, 7689–7696.

(31) Hagen, A.; Hertel, T. Quantitative Analysis of Optical Spectra from Individual Single-Wall Carbon Nanotubes. *Nano Lett.* **2003,** *3*, 383–388.

(32) Sen, R.; Rickard, S. M.; Itkis, M. E.; Haddon, R. C. Controlled Purification of Single-Walled Carbon Nanotube Films by Use of Selective Oxidation and near-IR Spectroscopy. *Chem. Mater.* **2003,** *15*, 4273–4279.

(33) Landi, B. J.; Ruf, H. J.; Evans, C. M.; Cress, C. D.; Raffaelle, R. P. Purity Assessment of Single-Wall Carbon Nanotubes, Using Optical Absorption Spectroscopy. *J. Phys. Chem. B* **2005,** *109*, 9952–9965.

(34) Saito, R.; Dresselhaus, G.; Dresselhaus, M. S. Trigonal Warping Effect of Carbon Nanotubes. *Phys. Rev. B* **2000,** *61*, 2981–2990.





DOI: 10.1021/jz100161p | *J. Phys. Chem. Lett.* **2010,** *1*, 1143–1148